Highlights

Exact Constraint Enforcement in Physics-Informed Extreme Learning Machines using Null-Space Projection Framework

Rishi Mishra, Smriti, Balaji Srinivasan, Sundararajan Natarajan, Ganapathy Krishnamurthi

- Introduces a projection framework achieving exact enforcement of linear constraints through algebraic operations in coefficient space.
- Transforms constrained optimization into unconstrained minimization by restricting to admissible coefficient manifolds.
- Eliminates penalty parameters and problem-specific constructions while extending to arbitrary geometries.
- Validates through experiments spanning multiple dimensions including complex geometries and coupled systems.

Exact Constraint Enforcement in Physics-Informed Extreme Learning Machines using Null-Space Projection Framework

Rishi Mishra[a,*], Smriti[b], Balaji Srinivasan[c], Sundararajan Natarajan[b,1], Ganapathy Krishnamurthi[c]

[a]*Department of Engineering Design, Indian Institute of Technology Madras, Chennai, 600036, Tamil Nadu, India*
[b]*Department of Mechanical Engineering, Indian Institute of Technology Madras, Chennai, 600036, Tamil Nadu, India*
[c]*Wadhwani School of Data Science & AI, Indian Institute of Technology Madras, Chennai, 600036, Tamil Nadu, India*

Abstract

Physics-informed extreme learning machines (PIELMs) typically impose boundary and initial conditions through penalty terms, yielding only approximate satisfaction that is sensitive to user-specified weights and can propagate errors into the interior solution. This work introduces Null-Space Projected PIELM (NP-PIELM), achieving exact constraint enforcement through algebraic projection in coefficient space. The method exploits the geometric structure of the admissible coefficient manifold, recognizing that it admits a decomposition through the null space of the boundary operator. By characterizing this manifold via a translation-invariant representation and projecting onto the kernel component, optimization is restricted to constraint-preserving directions, transforming the constrained problem into unconstrained least-squares where boundary conditions are satisfied exactly at discrete collocation points. This eliminates penalty coefficients, dual variables, and problem-specific constructions while preserving single-shot training efficiency. Numerical experiments on elliptic and parabolic problems including complex geometries and mixed boundary conditions validate the framework.

Keywords: PIELM, exact constraint enforcement, Null-Space Projection

1. Introduction

Physics-informed machine learning and scientific machine learning have emerged as frameworks for solving systems governed by partial differential equations (PDEs), incorporating governing operators and constraint data into learning objectives. The physics-informed neural network (PINN) reformulates PDE problems as residual minimization tasks over neural network architectures, leveraging automatic differentiation [1], generating substantial subsequent research [2–4]. Physics-Informed Extreme Learning Machines (PIELMs) retain physics-guided residual minimization while substituting iterative gradient-based optimization with randomized feature mapping and direct linear solves for output weights [5]. This enables single-shot training, with favorable computational scaling demonstrated across elliptic, parabolic, and inverse problems [6–10]. The ELM-based PDE literature includes constrained least-squares variants with convergence analysis [11, 12], local and domain-decomposition formulations [13–15], improved training strategies [13, 16], polynomial and

*Corresponding author
[1]Pandurangan Faculty Fellow

kernel-based networks [17–22], eigenvalue problems [23] and hierarchical, distributed, and problem-specific architectures [8, 24–27].

In physics-informed approaches, boundary and initial conditions are commonly enforced as soft penalty terms in a composite loss function. While straightforward, this enforces constraints only in a least-squares sense, yielding approximate satisfaction. Multiple differently-scaled loss components produce gradient magnitude discrepancies during optimization, identified as a source of training instability [4, 28]. Adaptive optimizers and dynamic balancing schemes address this by rescaling loss contributions [4, 29–31], while other strategies target conditioning and variance reduction [32–34]. Despite these advances, constraint satisfaction remains approximate, and residual mismatch can propagate errors into interior solutions, particularly for boundary layers, stiff dynamics, or constraint-sensitive problems [35, 36]. Penalty weight selection remains problem-dependent without principled guidance.

An alternative family enforces constraints exactly by embedding them into the trial solution ansatz, decoupling constraint satisfaction from residual minimization. The classical construction expresses the trial solution as $u_{\text{trial}}(x) = A(x) + B(x)N(x;\theta)$, where $A(x)$ satisfies prescribed data exactly and $B(x)$ vanishes on the constraint manifold [37, 38]. This guarantees exact enforcement but requires problem-specific derivations that become complex for mixed conditions and irregular geometries. McFall and Mahan used thin-plate spline interpolants to encode boundary distances [39]. Sukumar and Srivastava [40] multiplied network outputs by distance-function factors for Dirichlet enforcement, with extensions to Neumann and Robin conditions, though requiring accurate signed distance field computation. Berg and Nyström approximated geometry-dependent components via auxiliary networks, avoiding closed-form derivations but introducing two-stage training [41]. Recent hybrid architectures combine pre-trained networks and mixed-variable outputs for both Dirichlet and Neumann enforcement [42, 43]. Li et al. [44] proposed hard-constraint PINNs with multi-scale Fourier subnetworks for advection-diffusion equations.

The Theory of Functional Connections (TFC) embeds linear constraints into approximating ansatz by constructing constrained expressions: a function satisfying boundary constraints plus a projection of the free-function onto functions vanishing at constraints [45, 46]. Deep TFC uses neural networks as the free function [47], while Extreme TFC (X-TFC) pairs constrained expressions with ELM-style training [48]. However, constrained expressions become complex with increasing dimension and boundary complexity. Multivariate TFC is well-developed for rectangular domains, but extension to general geometries requires additional constructions [49]. Support function choices trivial in 1D require sophisticated strategies in higher dimensions, and constraint point counts grow with dimension and derivative order.

Another class treats constraints as explicit equality constraints within constrained optimization using Lagrange multipliers. Augmented Lagrangian PINNs [50] reformulate constraints through multipliers, solving min-max problems with adaptive balancing. This reduces boundary errors but achieves feasibility only up to optimization tolerance, with additional hyperparameters requiring tuning. Variational formulations enforce boundary conditions weakly through boundary integrals or Nitsche-type terms. The Deep Ritz method [51] optimizes energy functionals over neural network trial spaces, while variational PINNs [52] project residuals against test functions. Both inherit variational structure but achieve boundary consistency only in the weak sense.

Despite this diversity, each methodology faces limitations addressing exact constraint satisfaction

and practical applicability to multi-dimensional problems with complex geometries.

This work introduces Null-Space Projected PIELM (NP-PIELM), enforcing constraints exactly through algebraic projection rather than penalty formulations or iterative schemes. Unlike ansatz-based methods requiring problem-specific constraint-satisfying functions and distance-field computations, the approach operates in coefficient space through linear algebraic operations independent of domain geometry. The method exploits the geometric structure of the admissible coefficient manifold, recognizing that it admits a decomposition through the null space of the boundary operator. By characterizing this manifold via a translation-invariant representation and projecting onto the kernel component, optimization is restricted to constraint-preserving directions. This transforms constrained optimization into unconstrained least-squares minimization where physics residuals are evaluated on the admissible manifold.

The reduction eliminates auxiliary dual variables, penalty coefficient selection, and hyperparameter tuning, while ensuring constraints are met exactly at discrete boundary points. Constraint satisfaction remains independent of interior residual minimization. Unlike TFC where expressions become complex with dimension and geometry, the projection operates uniformly across arbitrary geometries and scales naturally to higher dimensions. The framework provides exact enforcement through a dimension-independent mechanism applicable to irregular domains, inheriting single-shot ELM efficiency and classical constrained least-squares stability [53–55].

The primary contributions include:

- A novel NP-PIELM framework enforcing linear boundary and initial conditions exactly through algebraic operations in coefficient space.
- Reformulation as unconstrained least-squares over a reduced coefficient space, where constraint satisfaction is guaranteed independent of residual minimization.
- Elimination of dual variables, penalty parameters, and problem-specific constructions including constraint-satisfying functions and distance-field computations.
- A geometrically flexible, dimensionally scalable approach extending to arbitrary domains while maintaining exact enforcement and computational efficiency.
- Numerical validation across elliptic and parabolic problems in multiple dimensions demonstrating exact boundary enforcement and superior accuracy.

In what follows, Section 2 reviews Physics-Informed Extreme Learning Machines including the mathematical setup and penalty-based constraint enforcement. Section 3 introduces NP-PIELM with the algebraic formulation and projected residual minimization. Section 4 demonstrates the framework through numerical examples, followed by conclusions.

2. Physics-Informed Extreme Learning Machine Overview

The physics-informed extreme learning machine (PIELM) framework combines the computational structure of extreme learning machines [56–59] with physics-based residual minimization principles. The method constructs a surrogate model satisfying governing physical laws without iterative backpropagation. PIELM employs a single hidden layer network where the weight vectors $\{\mathbf{w}_k\}_{k=1}^{N_\phi} \subset \mathbb{R}^d$ and biases $\{b_k\}_{k=1}^{N_\phi} \subset \mathbb{R}$ of the hidden layer are randomly initialized and remain fixed throughout

training(see Figure 1). This fixed random feature representation transforms the problem into finding optimal linear combinations of features approximating the target field. Since only output weights require determination, the solution is obtained directly through linear solvers, eliminating gradient-based iterative optimization [5].

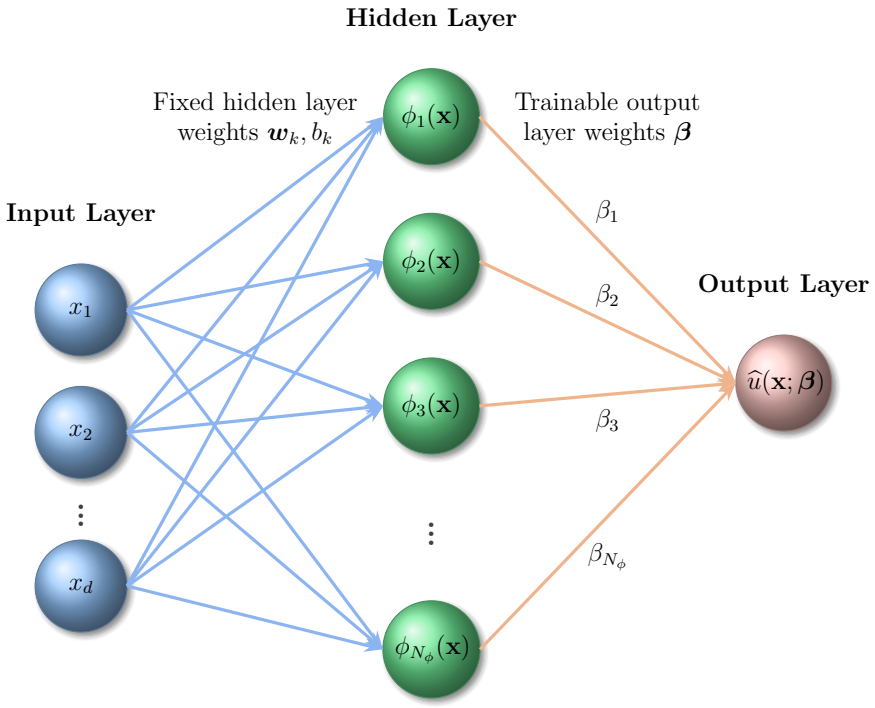

Figure 1: Schematic representation of the Physics-Informed Extreme Learning Machine (PIELM) architecture

Let $\Omega \subset \mathbb{R}^d$ denote a bounded spatial domain with boundary $\partial\Omega$. The physical system is described by a linear differential operator $\mathcal{L}$ and boundary operator $\mathcal{B}$:

$$\mathcal{L}u(\mathbf{x}) = f(\mathbf{x}) \text{ for } \mathbf{x} \in \Omega, \quad \mathcal{B}u(\mathbf{x}^b) = g(\mathbf{x}^b) \text{ for } \mathbf{x}^b \in \partial\Omega, \tag{1}$$

where $f(\mathbf{x})$ is the source term and $g(\mathbf{x}^b)$ specifies boundary data. The PIELM solution ansatz is

$$\widehat{u}(\mathbf{x};\boldsymbol{\beta}) = \sum_{k=1}^{N_\phi} \beta_k \sigma(\mathbf{w}_k^\top \mathbf{x} + b_k) = \boldsymbol{\phi}(\mathbf{x})^\top \boldsymbol{\beta}, \tag{2}$$

where $\boldsymbol{\phi}(\mathbf{x}) = [\sigma(\mathbf{w}_1^\top \mathbf{x} + b_1), \ldots, \sigma(\mathbf{w}_{N_\phi}^\top \mathbf{x} + b_{N_\phi})]^\top \in \mathbb{R}^{N_\phi}$ represents the fixed basis functions and $\boldsymbol{\beta} \in \mathbb{R}^{N_\phi}$ denotes the trainable output layer coefficients.

Sampling N_x interior collocation points $\{\mathbf{x}_i\}_{i=1}^{N_x} \subset \Omega$ and N_b boundary points $\{\mathbf{x}_j^b\}_{j=1}^{N_b} \subset \partial\Omega$, the differential and boundary sampling matrices are constructed as

$$\boldsymbol{\Psi} = \begin{bmatrix} (\mathcal{L}\boldsymbol{\phi}(\mathbf{x}_1))^\top \\ \vdots \\ (\mathcal{L}\boldsymbol{\phi}(\mathbf{x}_{N_x}))^\top \end{bmatrix} \in \mathbb{R}^{N_x \times N_\phi}, \quad \mathbf{B}_{bc} = \begin{bmatrix} (\mathcal{B}\boldsymbol{\phi}(\mathbf{x}_1^b))^\top \\ \vdots \\ (\mathcal{B}\boldsymbol{\phi}(\mathbf{x}_{N_b}^b))^\top \end{bmatrix} \in \mathbb{R}^{N_b \times N_\phi}. \tag{3}$$

The corresponding target vectors are $\mathbf{f} = [f(\mathbf{x}_1), \ldots, f(\mathbf{x}_{N_x})]^\top \in \mathbb{R}^{N_x}$ and $\mathbf{g} = [g(\mathbf{x}_1^b), \ldots, g(\mathbf{x}_{N_b}^b)]^\top \in \mathbb{R}^{N_b}$. The combined stacked system matrix and target vector are

$$\boldsymbol{\mathcal{X}} = \begin{bmatrix} \boldsymbol{\Psi} \\ \mathbf{B}_{bc} \end{bmatrix} \in \mathbb{R}^{(N_x+N_b)\times N_\phi}, \qquad \boldsymbol{\mathcal{Y}} = \begin{bmatrix} \mathbf{f} \\ \mathbf{g} \end{bmatrix} \in \mathbb{R}^{N_x+N_b}. \tag{4}$$

The physics-informed least-squares objective becomes

$$J(\boldsymbol{\beta}) = \frac{1}{2}\|\boldsymbol{\mathcal{X}}\boldsymbol{\beta} - \boldsymbol{\mathcal{Y}}\|_2^2. \tag{5}$$

The stationarity condition $\nabla_{\boldsymbol{\beta}} J = \mathbf{0}$ yields the normal equations $\boldsymbol{\mathcal{X}}^\top \boldsymbol{\mathcal{X}}\boldsymbol{\beta} = \boldsymbol{\mathcal{X}}^\top \boldsymbol{\mathcal{Y}}$. The canonical least-squares solution is expressed using the Moore-Penrose pseudoinverse as

$$\boldsymbol{\beta}^\star = \boldsymbol{\mathcal{X}}^\dagger \boldsymbol{\mathcal{Y}}, \tag{6}$$

which minimizes $\|\boldsymbol{\mathcal{X}}\boldsymbol{\beta} - \boldsymbol{\mathcal{Y}}\|_2^2$ and has the smallest Euclidean norm among all minimizers. For ill-conditioned systems, Tikhonov regularization $\boldsymbol{\beta}_\varepsilon = (\boldsymbol{\mathcal{X}}^\top \boldsymbol{\mathcal{X}} + \varepsilon \mathbf{I})^{-1} \boldsymbol{\mathcal{X}}^\top \boldsymbol{\mathcal{Y}}$ provides stable solutions.

3. Constraint Enforcement via Null Space Projection

In this section, we introduce the Null Space Projected PIELM (NP-PIELM), which achieves exact constraint enforcement through algebraic reparameterization. The method exploits the geometric structure of coefficient sets satisfying the discrete constraint system.

3.1. Admissible Coefficient Manifold Characterization

The boundary constraint system $\mathbf{B}_{bc}\boldsymbol{\beta} = \boldsymbol{g}$ defines an admissible set in coefficient space. Let $\mathcal{S}_{\text{adm}} \subset \mathbb{R}^{N_\phi}$ denote this set. The geometric structure of $\mathcal{S}_{\text{adm}}$ admits a decomposition through the null space structure of $\mathbf{B}_{bc}$.

Consider the projection operator $\mathcal{P}_{\mathcal{N}} : \mathbb{R}^{N_\phi} \to \ker(\mathbf{B}_{bc})$ that maps onto the null space of the boundary operator. For any $\boldsymbol{\beta} \in \mathcal{S}_{\text{adm}}$, the null space projection satisfies the invariance property

$$\mathcal{P}_{\mathcal{N}}(\boldsymbol{\beta} - \boldsymbol{\beta}_\star) = \boldsymbol{\beta} - \boldsymbol{\beta}_\star \quad \text{for all } \boldsymbol{\beta} \in \mathcal{S}_{\text{adm}}. \tag{7}$$

The admissible manifold can be characterized through a translation-invariant representation. Let $\boldsymbol{\beta}_\star$ be any element satisfying the constraint equation. If $\boldsymbol{\beta}_\star$ satisfies $\mathbf{B}_{bc}\boldsymbol{\beta}_\star = \boldsymbol{g}$, then the difference set satisfies

$$\mathcal{S}_{\text{adm}} - \boldsymbol{\beta}_\star = \ker(\mathbf{B}_{bc}), \tag{8}$$

establishing that $\mathcal{S}_{\text{adm}}$ is an affine subspace whose translational component coincides with the kernel of the boundary operator.

The fundamental theorem of linear algebra provides the orthogonal decomposition $\mathbb{R}^{N_\phi} = \ker(\mathbf{B}_{bc}) \oplus \mathcal{R}(\mathbf{B}_{bc}^\top)$, where $\mathcal{R}(\cdot)$ denotes the range. Define the complementary projection $\mathcal{P}_{\mathcal{R}} = \mathcal{I} - \mathcal{P}_{\mathcal{N}}$ projecting onto $\mathcal{R}(\mathbf{B}_{bc}^\top)$. This decomposition induces a natural splitting of the coefficient space into constraint-preserving and constraint-violating components.

3.2. Projected Residual Minimization on the Admissible Manifold

The physics residual minimization is restricted to $\mathcal{S}_{\text{adm}}$ through the null space projection. Let $\mathbf{W} \in \mathbb{R}^{N_\phi \times m}$ be a matrix whose columns span the tangent space (kernel component) of $\mathcal{S}_{\text{adm}}$ at any point, where $m = \dim(\mathcal{S}_{\text{adm}})$. The projection structure implies that any admissible coefficient vector admits the representation

$$\boldsymbol{\beta} = \boldsymbol{\beta}_\star + \mathbf{W}\boldsymbol{\eta}, \quad \boldsymbol{\eta} \in \mathbb{R}^m. \tag{9}$$

The constraint equation is automatically satisfied for all $\boldsymbol{\eta}$ by construction of $\mathbf{W}$.

Substituting into the physics residual and applying the null space projection yields the transformed objective

$$\tilde{J}(\boldsymbol{\eta}) = \|\boldsymbol{\Psi}(\boldsymbol{\beta}_\star + \mathbf{W}\boldsymbol{\eta}) - \mathbf{f}\|_2^2 = \|\tilde{\boldsymbol{\Psi}}\boldsymbol{\eta} - \tilde{\mathbf{f}}\|_2^2, \tag{10}$$

where the reduced quantities $\tilde{\boldsymbol{\Psi}} \in \mathbb{R}^{N_x \times m}$ and $\tilde{\mathbf{f}} \in \mathbb{R}^{N_x}$ are derived from the original system through the manifold parameterization.

The minimization over $\boldsymbol{\eta}$ proceeds via standard least-squares techniques on the projected system. The optimal $\boldsymbol{\eta}^\star$ satisfies the reduced normal equations

$$\tilde{\boldsymbol{\Psi}}^\top \tilde{\boldsymbol{\Psi}}\, \boldsymbol{\eta} = \tilde{\boldsymbol{\Psi}}^\top \tilde{\mathbf{f}}, \tag{11}$$

with the final coefficient vector recovered as $\boldsymbol{\beta}^\star = \boldsymbol{\beta}_\star + \mathbf{W}\boldsymbol{\eta}^\star$.

The key properties of the null space projection framework are: (i) constraint satisfaction is independent of interior residual minimization (ii) the reduced dimension m preserves approximation capacity for admissible solutions (iii) the projection framework extends naturally to mixed constraints, complex geometries, and coupled systems.

4. Numerical Examples

We assess the performance of NP-PIELM on a representative set of benchmark problems including steady elliptic equations, unsteady parabolic problems in space-time formulations, problems on complex geometries, and coupled velocity-pressure systems. These tests evaluate how accurately NP-PIELM resolves smooth solutions, handles transport and diffusion phenomena, and manages complex geometries within a unified formulation.

In all examples, NP-PIELM employs Bernstein polynomials as basis functions. For one-dimensional problems, we use $(d+1)$ Bernstein polynomials of degree d. For higher-dimensional and space-time problems, tensor-product Bernstein bases are constructed in the relevant coordinates. Interior collocation points are sampled uniformly, and for non-standard domains, points are restricted to the physical region. All computations are performed in MATLAB R2023b using double precision arithmetic on an Intel Core i9-13980HX (2.20 GHz) processor with 32 GB RAM.

4.1. 1D Steady Convection-Diffusion-Reaction

We consider a one-dimensional steady convection-diffusion-reaction problem with strong advection and small diffusion coefficient $\nu = 10^{-3}$:

$$-\nu\, u''(x) + 2(2x-1)\, u'(x) + 4\, u(x) = 0, \quad x \in [0,1]. \tag{12}$$

Due to the dominance of convective and reactive terms over diffusion, the solution exhibits boundary-layer behavior near the domain ends. The exact analytical solution is

$$u_{\text{ex}}(x) = \exp\left(\frac{2}{\nu}(x^2 - x)\right), \tag{13}$$

with Dirichlet boundary conditions $u(0) = u_{\text{ex}}(0)$ and $u(1) = u_{\text{ex}}(1)$.

A total of $N_\phi = 501$ neurons (Bernstein basis) is used to capture the steep gradients. The PDE residual is evaluated at $N_x = 1000$ uniformly distributed interior points. The computation time is 0.138s. Figure 2(a) compares the NP-PIELM solution with the exact profile evaluated at 100 uniformly sampled test points. The two curves are visually identical even in the narrow boundary layers. The maximum absolute error on the test set is 4.389×10^{-9}, with pointwise errors shown in Figure 2(b) remaining below 10^{-9} across the domain.

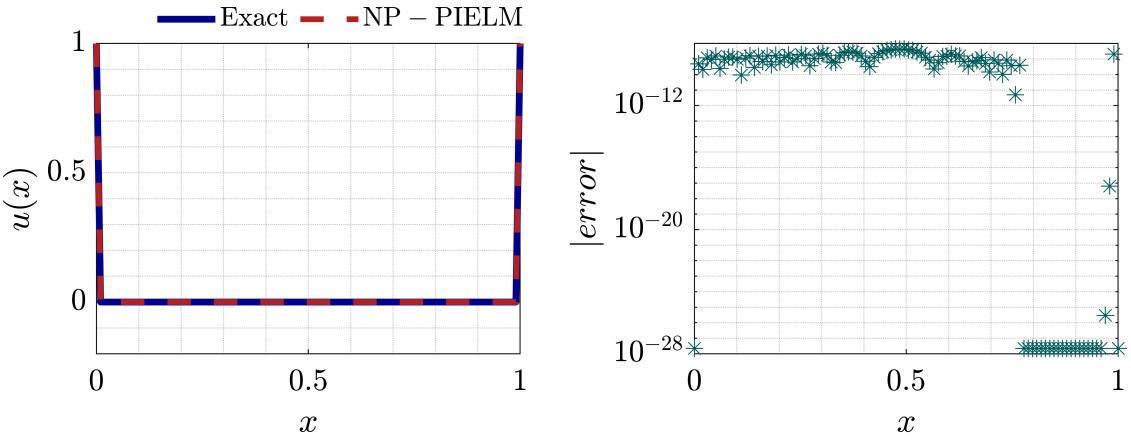

(a) Exact vs NP-PIELM

(b) Absolute Error

Figure 2: 1D steady convection-diffusion-reaction problem: (a) comparison of exact and NP-PIELM solutions showing boundary-layer behavior, (b) pointwise absolute error.

4.2. 1D Unsteady Advection-Diffusion

We consider an unsteady advection-diffusion problem to demonstrate NP-PIELM for space-time formulations. The time coordinate is treated as an additional dimension, allowing direct solution over the entire space-time domain:

$$u_t(x,t) + c\,u_x(x,t) - \kappa\,u_{xx}(x,t) = f(x,t), \quad (x,t) \in [0,1] \times [0,1], \tag{14}$$

where $c = 1.0$ is the advection velocity and $\kappa = 0.05$ is the diffusion coefficient. The exact solution is

$$u_{\text{ex}}(x,t) = \sin\left(2\pi(x - ct)\right) e^{-\alpha t}, \tag{15}$$

with $\alpha = 0.5$ controlling temporal decay. Boundary conditions at $x = 0, 1$ and the initial condition at $t = 0$ are prescribed from the exact solution.

The space-time approximation uses a tensor-product Bernstein basis with degrees $d_x = d_t = 20$, giving $N_\phi = 441$ neurons. The PDE residual is evaluated at $45 \times 45 = 2025$ interior points, with boundary and initial conditions enforced through 135 constraint rows. Computation time is 0.086s.

Figure 3 shows results at $t = 0, 0.3, 0.6$. The solution exhibits smooth advective transport with diffusive damping. Maximum absolute errors on the test grid are 2.11×10^{-15} at $t = 0$, 4.33×10^{-15} at $t = 0.3$, and 2.44×10^{-15} at $t = 0.6$, with pointwise errors in the range $10^{-16} - 10^{-15}$.

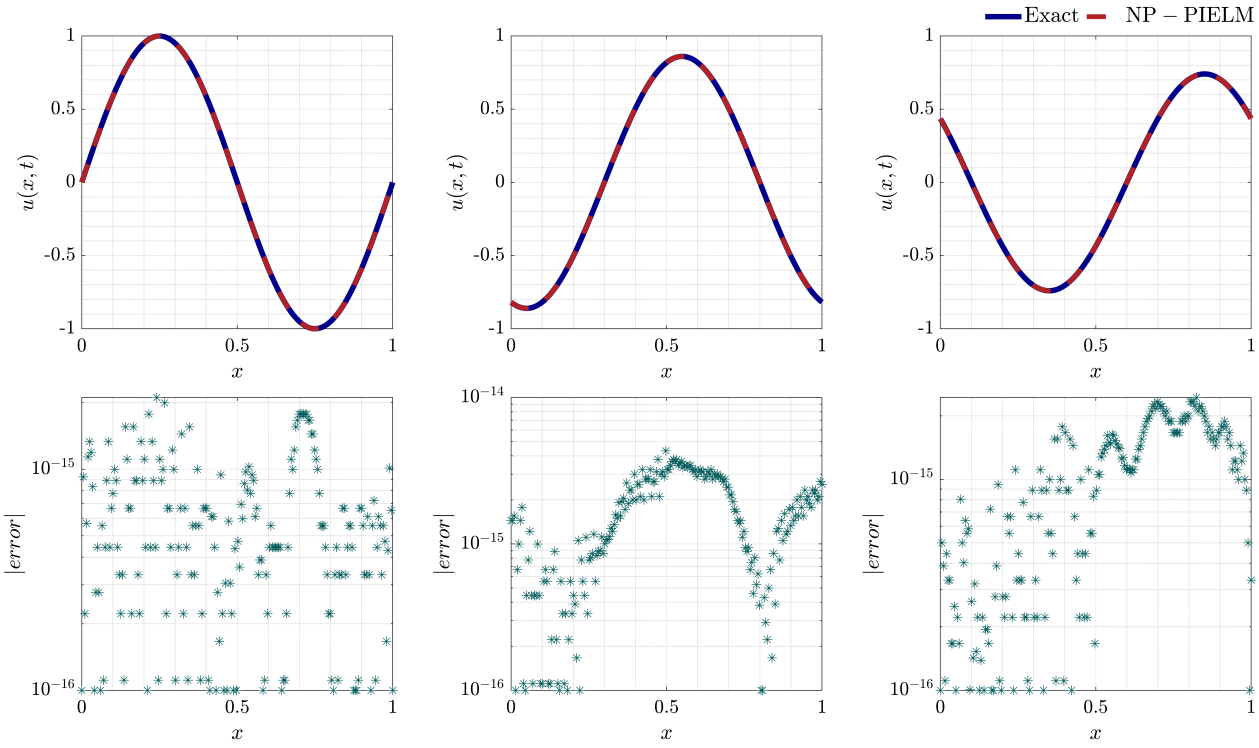

(a) t = 0 (b) t = 0.3 (c) t = 0.6

Figure 3: 1D unsteady advection-diffusion problem solved in space-time form. (a-c) Comparison of the exact and NP-PIELM solutions at (t = 0, 0.3, 0.6) showing advective transport with temporal decay. Bottom row shows corresponding pointwise absolute error at each time level.

4.3. 2D Poisson with Mixed Boundary Conditions

We consider a two-dimensional Poisson problem on the unit square $\Omega = [0, 1]^2$:

$$u_{xx}(x, y) + u_{yy}(x, y) = (2 - \pi^2 y^2) \sin(\pi x), \quad (x, y) \in [0, 1] \times [0, 1]. \tag{16}$$

The exact solution is $u_{\text{ex}}(x, y) = y^2 \sin(\pi x)$. Homogeneous Dirichlet conditions are imposed on three boundaries: $u(0, y) = 0$, $u(1, y) = 0$, $u(x, 0) = 0$, while a non-homogeneous Neumann condition is prescribed on the top boundary: $u_y(x, 1) = 2 \sin(\pi x)$.

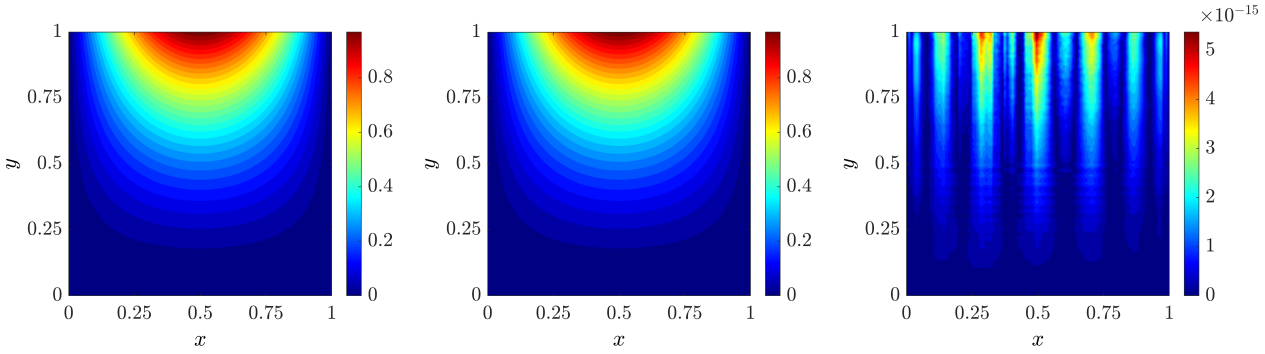

(a) Exact Solution (b) NP-PIELM Solution (c) Absolute Error

Figure 4: 2D Poisson problem with mixed boundary conditions: (a) exact solution, (b) NP-PIELM solution, (c) pointwise absolute error on 100×100 test grid.

The numerical solution uses a tensor-product Bernstein basis with $d_x = d_y = 15$, giving $N_\phi = 256$ neurons. The PDE residual is evaluated at $30 \times 30 = 900$ interior points, with boundary conditions sampled at 30 points per edge (120 constraint rows). Computation time is 0.07s. Figure 4 shows results on a 100×100 test grid. The exact and NP-PIELM contours are visually identical. The maximum absolute error is 5.55×10^{-15}, with errors uniformly in the range $10^{-16} - 10^{-15}$.

4.4. 2D Unsteady Heat on Flower Domain

We consider unsteady heat conduction on a non-standard flower-shaped domain Ω_{flower} defined by $r(\theta) = R_0 + a\sin(m\theta)$ with $R_0 = 0.5$, $a = 0.2$, and $m = 5$ petals:

$$T_t(x, y, t) - \alpha \Delta T(x, y, t) = f(x, y, t), \quad (x, y, t) \in \Omega_{\text{flower}} \times [0, 1], \tag{17}$$

with thermal diffusivity $\alpha = 0.01$. The exact solution is a Gaussian profile with exponential temporal decay:

$$T_{\text{ex}}(x, y, t) = \exp\left(- \frac{x^2 + y^2}{2\sigma^2} \right) \exp(-\beta t), \tag{18}$$

with $\sigma = 0.5$ and $\beta = 1.0$. Dirichlet conditions are prescribed on the flower boundary, with initial condition at $t = 0$.

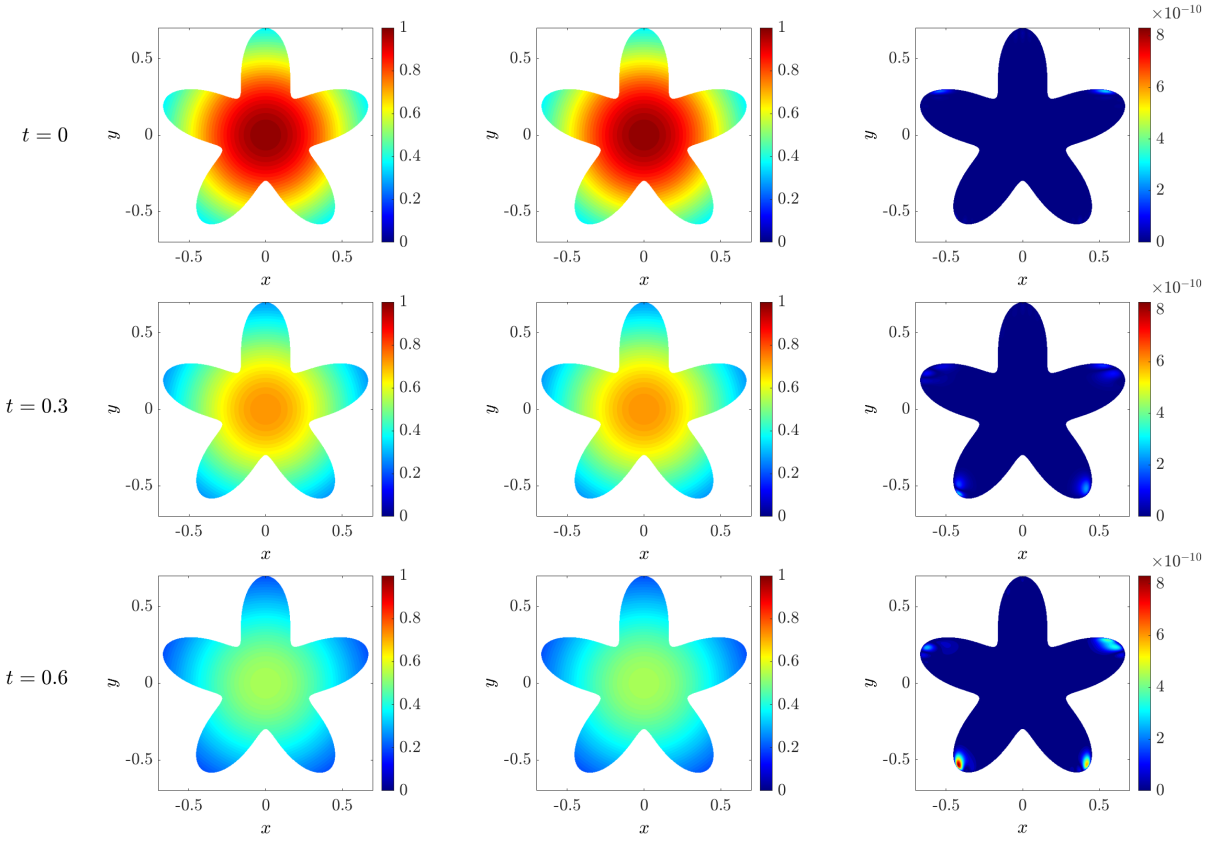

(a) Exact Solution (b) NP-PIELM Solution (c) Absolute Error

Figure 5: 2D unsteady heat conduction on flower-shaped domain ($\alpha = 0.01$) at $t = 0, 0.3, 0.6$: (a) exact temperature, (b) NP-PIELM prediction, (c) pointwise absolute error.

A tensor-product Bernstein basis with $d_x = d_y = 18$ and $d_t = 12$ gives $N_\phi = 4693$ neurons. Interior collocation uses 7680 space-time points within the flower region, with 4384 constraint rows for boundary and initial conditions. Computation time is 19.39s. Figure 5 shows results on a 500×500 test grid (107,758 interior points) at $t = 0, 0.3, 0.6$. The exact and NP-PIELM fields are visually indistinguishable. Maximum absolute errors are 2.88×10^{-10} at $t = 0$, 2.81×10^{-10} at $t = 0.3$, and 8.31×10^{-10} at $t = 0.6$.

4.5. 2D Steady Stokes Flow

We consider steady incompressible Stokes flow on $\Omega = [0, 2\pi] \times [0, 2\pi]$:

$$-\mu \Delta \boldsymbol{u}(x, y) + \nabla p(x, y) = \boldsymbol{f}(x, y), \quad \nabla \cdot \boldsymbol{u}(x, y) = 0, \tag{19}$$

where $\boldsymbol{u} = (u_x, u_y)$ is velocity, p is pressure, and $\mu = 1$. A Taylor-Green manufactured solution is used:

$$u_x = \sin x \cos y, \quad u_y = -\cos x \sin y, \quad p = \tfrac{1}{4}(\cos 2x + \cos 2y). \tag{20}$$

Dirichlet velocity conditions are prescribed on $\partial\Omega$, with a pressure gauge $p(0, 0) = p_{\text{ex}}(0, 0)$ to fix the additive constant.

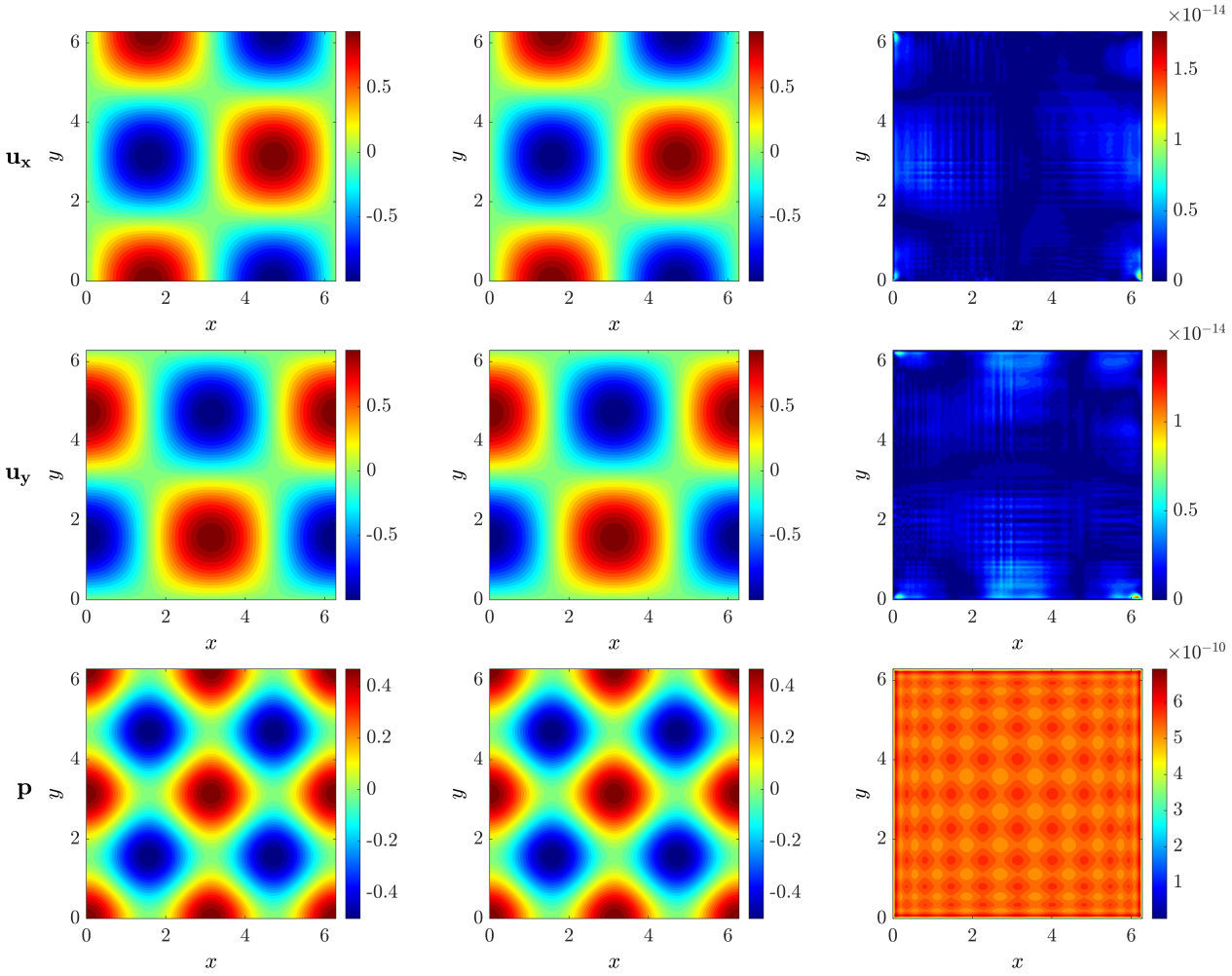

(a) Exact Solution (b) NP-PIELM Solution (c) Absolute Error

Figure 6: Steady 2D Stokes flow with Taylor-Green solution: (a) exact, (b) NP-PIELM, (c) absolute error for u_x (top), u_y (middle), p (bottom) on 100×100 test grid.

Each scalar field uses a tensor-product Bernstein basis with $d_x = d_y = 20$, giving $N_\phi = 441$ per field (1323 total coefficients). The PDE residual is evaluated at $50 \times 50 = 2500$ interior points. Boundary conditions contribute 400 scalar constraints plus one pressure gauge (401 constraint rows). Figure 6 shows results on a 100×100 test grid. The maximum absolute errors are 1.83×10^{-14} for u_x, 1.45×10^{-14} for u_y, and 7.16×10^{-10} for pressure. Both velocity components achieve machine precision, with pressure errors remaining small across the domain.

5. Conclusions

NP-PIELM achieves exact constraint enforcement through projection onto admissible coefficient manifolds. The framework transforms constrained problems into unconstrained optimization while preserving single-shot training efficiency. Numerical experiments demonstrate machine-precision accuracy across 1D-2D problems, complex geometries, and coupled systems. The approach eliminates penalty tuning and problem-specific constructions, providing a unified mechanism for constraint enforcement in physics-informed learning.

Future work includes extending the framework to nonlinear problems and inverse settings, analyzing conditioning for larger systems, and exploring combinations with adaptive sampling and domain decomposition. Broader comparisons with other physics-informed methods would further establish the practical utility of NP-PIELM.

References

[1] M. Raissi, P. Perdikaris, G. E. Karniadakis, Physics-informed neural networks: A deep learning framework for solving forward and inverse problems involving nonlinear partial differential equations, Journal of Computational Physics 378 (2019) 686–707. doi:10.1016/j.jcp.2018.10.045.
URL https://doi.org/10.1016/j.jcp.2018.10.045

[2] Z. K. Lawal, H. Yassin, D. T. C. Lai, A. Che Idris, Physics-informed neural network (pinn) evolution and beyond: A systematic literature review and bibliometric analysis, Big Data and Cognitive Computing 6 (4) (2022) 140.

[3] K. Luo, J. Zhao, Y. Wang, J. Li, J. Wen, J. Liang, H. Soekmadji, S. Liao, Physics-informed neural networks for pde problems: A comprehensive review, Artificial Intelligence Review 58 (10) (2025) 1–43.

[4] S. Wang, Y. Teng, P. Perdikaris, Understanding and mitigating gradient flow pathologies in physics-informed neural networks, SIAM Journal on Scientific Computing 43 (5) (2021) A3055–A3081.

[5] V. Dwivedi, B. Srinivasan, Physics-informed extreme learning machine (PIELM), Neurocomputing 399 (2020) 193–210. doi:10.1016/j.neucom.2020.02.064.
URL https://doi.org/10.1016/j.neucom.2020.02.064

[6] S. Zeng, Y. Liang, Q. Zhang, High-precision physics-informed extreme learning machines for evolving interface problems, Engineering Analysis with Boundary Elements 174 (2025) 106171.

[7] V. Dwivedi, B. Srinivasan, M. Sigovan, B. Sixou, Kernel-adaptive pi-elms for forward and inverse problems in pdes with sharp gradients, arXiv preprint arXiv:2507.10241 (2025).

[8] V. Dwivedi, B. Srinivasan, Solution of biharmonic equation in complicated geometries with physics informed extreme learning machine, Journal of Computing and Information Science in Engineering 20 (6) (2020).

[9] S. Rout, V. Dwivedi, B. Srinivasan, Numerical approximation in cfd problems using physics informed machine learning, arXiv preprint arXiv:2111.02987 (2021).

[10] Q. Wang, C. Li, S. Zhang, C. Zhou, Y. Zhou, Physics-informed extreme learning machine framework for solving linear elasticity mechanics problems, International Journal of Solids and Structures 309 (2025) 113157.

[11] D. E. De Falco, F. Calabro, M. Pragliola, Insights on the different convergences in extreme learning machine, Neurocomputing 599 (2024) 128061.

[12] D. E. De Falco, E. Schiassi, F. Calabrò, Least squares with equality constraints extreme learning machines for the resolution of PDEs, arXiv preprint arXiv:2503.19185Available at arXiv:2503.19185 (2025).

[13] S. Dong, Z. Li, A modified batch intrinsic plasticity method for pre-training the random coefficients of extreme learning machines, Journal of Computational Physics 445 (2021) 110585.

[14] F. Calabrò, G. Fabiani, C. I. Siettos, Extreme learning machine collocation for the numerical solution of elliptic PDEs with sharp gradients, Computer Methods in Applied Mechanics and Engineering 387 (2021) 114188. doi:10.1016/j.cma.2021.114188.

[15] Y. Liang, Q. Zhang, S. Zeng, A piecewise extreme learning machine for interface problems, Mathematics and Computers in Simulation 227 (2025) 303–321.

[16] S. Dong, J. Yang, On computing the hyperparameter of extreme learning machines: Algorithm and application to computational PDEs, and comparison with classical and high-order finite elements, Journal of Computational Physics 463 (2022) 111290. doi:10.1016/j.jcp.2022.111290.

[17] Y. Yang, M. Hou, J. Luo, A novel improved extreme learning machine algorithm in solving ordinary differential equations by legendre neural network methods, Advances in Difference Equations 2018 (2018) 469.

[18] H. Sun, M. Hou, Y. Yang, T. Zhang, F. Weng, F. Han, Solving partial differential equation based on bernstein neural network and extreme learning machine algorithm, Neural Processing Letters 50 (2019) 1153–1172. doi:10.1007/s11063-018-9911-8.

[19] H. Liu, B. Xing, Z. Wang, L. Li, Legendre neural network method for several classes of singularly perturbed differential equations based on mapping and piecewise optimization technology, Neural Processing Letters 51 (2020) 2891–2913. doi:10.1007/s11063-020-10232-9.

[20] M. Liu, M. Hou, J. Wang, Y. Cheng, Solving two-dimensional linear partial differential equations based on chebyshev neural network with extreme learning machine algorithm, Engineering Computations 38 (2021) 874–894. doi:10.1108/EC-08-2019-0387.

[21] Y. Yang, M. Hou, H. Sun, T. Zhang, F. Weng, J. Luo, Neural network algorithm based on legendre improved extreme learning machine for solving elliptic partial differential equations, Soft Computing 24 (2020) 1083–1096.

[22] S. Li, G. Liu, S. Xiao, Extreme learning machine with kernels for solving elliptic partial differential equations, Cognitive Computation 15 (2023) 413–428.

[23] R. Mishra, Smriti, G. Krishnamurthi, B. Srinivasan, S. Natarajan, Eig-pielm: an efficient mesh-free method for eigenvalue problems using physics-informed extreme learning machines, Computer Methods in Applied Mechanics and Engineering 451 (2026) 118674. doi:https://doi.org/10.1016/j.cma.2025.118674.
URL https://www.sciencedirect.com/science/article/pii/S0045782525009466

[24] D. Dong, J. Kou, W. Suo, W. Zhang, Hierarchical extreme learning machine for solving partial differential equations, Available at SSRN 4775113 (2024).

[25] V. Dwivedi, N. Parashar, B. Srinivasan, Distributed learning machines for solving forward and inverse problems in partial differential equations, Neurocomputing 420 (2021) 299–316.

[26] X.-A. Li, J. Wu, Z. Ding, X. Tai, L. Liu, Y.-G. Wang, Extreme learning machine-assisted solution of biharmonic equations via its coupled schemes (2024).

[27] G. Fabiani, F. Calabrò, L. Russo, C. Siettos, Numerical solution and bifurcation analysis of nonlinear partial differential equations with extreme learning machines, Journal of Scientific Computing 89 (2021) 44.

[28] S. Wang, X. Yu, P. Perdikaris, When and why PINNs fail to train: A neural tangent kernel perspective, Journal of Computational Physics 449 (2022) 110768. arXiv:2007.14527, doi:10.1016/j.jcp.2021.110768.
URL https://doi.org/10.1016/j.jcp.2021.110768

[29] S. Li, X. Feng, Dynamic weight strategy of physics-informed neural networks for the 2d navier–stokes equations, Entropy 24 (9) (2022) 1254.

[30] L. D. McClenny, U. M. Braga-Neto, Self-adaptive physics-informed neural networks, Journal of Computational Physics 474 (2023) 111722.

[31] Z. Xiang, W. Peng, X. Liu, W. Yao, Self-adaptive loss balanced physics-informed neural networks, Neurocomputing 496 (2022) 11–34.

[32] S. Regmi, B. Panthi, Y. Ming, P. K. Gyawali, D. Stoyanov, B. Bhattarai, Reweightood: Loss reweighting for distance-based ood detection, in: Proceedings of the IEEE/CVF Conference on Computer Vision and Pattern Recognition, 2024, pp. 131–141.

[33] M. Barreau, H. Shen, Accuracy and robustness of weight-balancing methods for training pinns, arXiv preprint arXiv:2501.18582 (2025).

[34] J. Hua, Y. Li, C. Liu, P. Wan, X. Liu, Physics-informed neural networks with weighted losses by uncertainty evaluation for accurate and stable prediction of manufacturing systems, IEEE Transactions on Neural Networks and Learning Systems 35 (8) (2023) 11064–11076.

[35] A. Krishnapriyan, A. Gholami, S. Zhe, R. Kirby, M. W. Mahoney, Characterizing possible failure modes in physics-informed neural networks, Advances in neural information processing systems 34 (2021) 26548–26560.

[36] S. Berrone, C. Canuto, M. Pintore, N. Sukumar, Enforcing dirichlet boundary conditions in physics-informed neural networks and variational physics-informed neural networks, Heliyon 9 (8) (2023).

[37] I. E. Lagaris, A. Likas, D. I. Fotiadis, Artificial neural network methods in quantum mechanics, Computer Physics Communications 104 (1-3) (1997) 1–14.

[38] I. E. Lagaris, A. Likas, D. I. Fotiadis, Artificial neural networks for solving ordinary and partial differential equations, IEEE Transactions on Neural Networks 9 (5) (1998) 987–1000. arXiv:physics/9705023, doi:10.1109/72.712178.
URL https://doi.org/10.1109/72.712178

[39] K. S. McFall, J. R. Mahan, Artificial neural network method for solution of boundary value problems with exact satisfaction of arbitrary boundary conditions, IEEE transactions on neural networks 20 (8) (2009) 1221–1233.

[40] N. Sukumar, A. Srivastava, Exact imposition of boundary conditions with distance functions in physics-informed deep neural networks, Computer Methods in Applied Mechanics and Engineering 389 (2022) 114333. arXiv:2104.08426, doi:10.1016/j.cma.2021.114333.
URL https://doi.org/10.1016/j.cma.2021.114333

[41] J. Berg, K. Nyström, A unified deep artificial neural network approach to partial differential equations in complex geometries, Neurocomputing 317 (2018) 28–41.

[42] C. Rao, H. Sun, Y. Liu, Physics-informed deep learning for computational elastodynamics without labeled data, Journal of Engineering Mechanics 147 (8) (2021) 04021043.

[43] S. Manavi, E. Fattahi, T. Becker, A trial solution for imposing boundary conditions of partial differential equations in physics-informed neural networks, Engineering Applications of Artificial Intelligence 127 (2024) 107236.

[44] X. Li, J. Deng, J. Wu, S. Zhang, W. Li, Y.-G. Wang, Physical informed neural networks with soft and hard boundary constraints for solving advection-diffusion equations using fourier expansions, Computers & Mathematics with Applications 159 (2024) 60–75.

[45] D. Mortari, The theory of connections: Connecting points, Mathematics 5 (4) (2017) 57.

[46] D. Mortari, C. Leake, The multivariate theory of connections, Mathematics 7 (3) (2019) 296.

[47] C. Leake, D. Mortari, Deep theory of functional connections: A new method for estimating the solutions of partial differential equations, Machine Learning and Knowledge Extraction 2 (1) (2020) 37–55. doi:10.3390/make2010004.
URL https://doi.org/10.3390/make2010004

[48] E. Schiassi, R. Furfaro, C. Leake, M. De Florio, H. Johnston, D. Mortari, Extreme theory of functional connections: A fast physics-informed neural network method for solving ordinary and partial differential equations, Neurocomputing 457 (2021) 334–356.

[49] D. Mortari, D. Arnas, Bijective mapping analysis to extend the theory of functional connections to non-rectangular 2-dimensional domains, Mathematics 8 (9) (2020) 1593.

[50] H. J. Son, J. Lee, E. Park, Al-PINNs: Augmented Lagrangian relaxation method for the training of physics-informed neural networks, Neurocomputing 544 (2023) 126246. arXiv:2205.01059, doi:10.1016/j.neucom.2023.126246.
URL https://doi.org/10.1016/j.neucom.2023.126246

[51] W. E, B. Yu, The deep ritz method: A deep learning-based numerical algorithm for solving variational problems, Communications in Mathematics and Statistics 6 (1) (2018) 1–12. doi:10.1007/s40304-018-0127-z.
URL https://doi.org/10.1007/s40304-018-0127-z

[52] E. Kharazmi, Z. Zhang, G. E. Karniadakis, hp-VPINNs: Variational physics-informed neural networks with domain decomposition, Computer Methods in Applied Mechanics and Engineering 374 (2021) 113547. doi:10.1016/j.cma.2020.113547.
URL https://doi.org/10.1016/j.cma.2020.113547

[53] A. J. Cox, N. J. Higham, Accuracy and stability of the null space method for solving the equality constrained least squares problem, Numerical Algorithms 22 (1) (1999) 23–44. doi:10.1023/A:1022365107361.
URL https://doi.org/10.1023/A:1022365107361

[54] C. L. Lawson, R. J. Hanson, Solving Least Squares Problems, Prentice-Hall, Englewood Cliffs, NJ, 1974.

[55] G. H. Golub, C. F. Van Loan, Matrix Computations, 4th Edition, Johns Hopkins University Press, Baltimore, MD, 2013.

[56] G.-B. Huang, Q.-Y. Zhu, C.-K. Siew, Extreme learning machine: theory and applications, Neurocomputing 70 (1-3) (2006) 489–501.

[57] G.-B. Huang, Q.-Y. Zhu, C.-K. Siew, Extreme learning machine: a new learning scheme of feedforward neural networks, in: 2004 IEEE international joint conference on neural networks (IEEE Cat. No. 04CH37541), Vol. 2, Ieee, 2004, pp. 985–990.

[58] G.-B. Huang, D. H. Wang, Y. Lan, Extreme learning machines: a survey, International journal of machine learning and cybernetics 2 (2) (2011) 107–122.

[59] G. Huang, G.-B. Huang, S. Song, K. You, Trends in extreme learning machines: A review, Neural Networks 61 (2015) 32–48.